A Highly Linear Single Balanced Mixer Based on Heterojunction Interband Tunneling Diode

Alessandro Cidronali, *Member, IEEE*, Giovanni Collodi, *Member, IEEE*, Mandar Ramesh Deshpande, *Member, IEEE*, Nada El-Zein, *Member, IEEE*, Vijay Nair, *Fellow, IEEE*, Gianfranco Manes, *Member, IEEE*, and Herb Goronkin, *Fellow, IEEE*

***Abstract*—In this paper, a compact and highly linear monolithic-microwave integrated circuit (MMIC) single balanced mixer based on heterojunction interband tunnel diode (HITD) technology working at 1.8 GHz is described. The prototype consists of a pair of HITDs biased at 0 V and a lumped-element directional coupler with arbitrary impedance terminations. The HITDs are in the InGaAs/InAlAs material system lattice matched to InP. The relevant feature of the mixer is the linearity due to the quasi-square-law dc current–voltage ($I\backslash V$) characteristics exhibited by the device around zero voltage. A qualitative treatment of the third-order intermodulation product and the conversion loss as a function of the HITDs $I\backslash V$ characteristic and the embedding impedance is provided. The design techniques along with a detailed experimental validation are also provided. The prototype working in down-conversion mode, exhibited an third-order intercept point power level of $+17.5$ dBm, a conversion loss of 11 dB and a 1-dB compression point of $+7$ dBm at the operative frequency of 1.8 GHz with a $+5$-dBm local-oscillator drive level.**

***Index Terms*—Linear mixer, microwave mixer, MMIC, quantum-well device.**

I. Introduction

THE increasing interest in personal communication systems (PCS), operating in the digital communications system (DCS)–1800 MHz and the industrial–scientific–medical (ISM) band (2.45 and 5.8 GHz), has stimulated research on low power consumption and compact and integrated multifunctional components. Low power consumption becomes an important topic, particularly for wireless applications, in order to conserve battery power, and to improve the talk time [1]. Zero-biased nonlinear elements become relevant in low-power circuit development. On the other hand, high-capacity microwave and millimeter-wave data links demand high capabilities in terms of dynamic range. It results in a severe requirement for intermodulation performance associated to the front-end mixer and, consequently, careful control and modeling of the device nonlinearity becomes necessary [2]–[5]. The availability of a novel technology such as heterojunction interband tunneling diodes (HITDs) enables the implementation of a new class of nonlinear element into monolithic-microwave integrated circuits (MMICs).

Manuscript received March 30, 2001; revised August 15, 2001.

A. Cidronali, G. Collodi, and G. Manes are with the Department of Electronics and Telecommunications, University of Florence, 3 I-50139 Florence, Italy (e-mail: acidronali@ingfi1.ing.unifi.it).

M. R. Deshpande, N. El-Zein, V. Nair, and H. Goronkin are with the Physical Sciences Research Laboratory, Motorola Laboratories, Tempe, AZ 85284 USA.

Publisher Item Identifier S 0018-9480(01)10445-X.

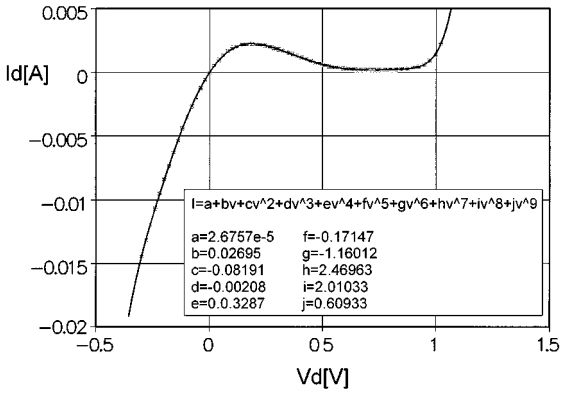

Fig. 1. HITD diode I/V characteristic that intrinsic behavior is approximated in the voltage range: $[-0.5$ V; 0.5 V] by a ninth degree polynomial.

High compactness is another important objective in PCS systems. Functional blocks, commonly used in transceiver RF sections [6]–[9], such as amplifiers, mixers, modulators, and phase shifters, make use of sub-circuits (power combiners, filters, matching networks, and directional couplers) designed by adopting a standard distributed elements approach. The monolithic implementation of such sub-circuits often results in large die area, owing to the dimensions of the transmission lines. High integration levels and compactness of these sub-circuits may be achieved by considering new circuit configurations based on a lumped-element approach [10], [11]. Furthermore, implementations of these circuits using passive elements would improve the power-handling capability and phase-noise characteristics of the communications system. Active configurations are generally very compact, and allow wide-band operations, but these implementations tend to increase the power consumption of circuits.

This paper presents a novel highly linear single balanced mixer based on 90° lumped element directional couplers (LEDCs) [12] and a pair of HITDs biased at 0 V. The quasi square-law behavior of their I/V characteristic of HITDs at $V = 0$ V (as seen in Fig. 1) enables the design of an efficient single balanced mixer. It is well known [13] that a nonlinearity of the nth degree generates nth-order mixing products. Consequently, the use of electron devices showing an approximately second degree nonlinearity in the mixer design allows an inherently good performance in terms of third-order intermodulation (IM3) products. HITDs appear to be more suitable than Schottky devices for mixers that have the unbiased junction impedance as the most dominant element [14]–[16]. In principle, the barrier layer thickness of

TABLE I
HITD LAYER STRUCTURE

p^+ - InGaAs	Top contact layer
nid - InAlAs	Barrier
nid - InGaAs	Quantum well
n^{++} - InAlAs	Bottom contact layer
n^+ - InGaAs	Ohmic contact layer
nid - InP	Substrate

HITDs can be tailored during device design in such a way that nonlinearities associated with the devices can be controlled to match the microwave signal pump requirements [15]. It is also possible, in principle, to choose either different layer structures or doping levels for a device of the same size to obtain optimum resistive nonlinearities. These are the main motivations for the investigation of the single balanced mixer, where the nonlinear elements are tunnel diodes biased at $Vd = 0$ V.

The paper is organized as follows. In Section II, the qualitative description of a tunnel-diode-based mixer is revisited and the performance in terms of the IM3 product and conversion loss are related to the resistive diode's nonlinearity. In Section III, the design technique of the balanced mixer is then depicted with a major emphasis on the design of an arbitrary embedding impedance value. A discussion of the performance sensitivity to this latter parameter is given. The conversion loss dependence from the HITDs peak current is then shown with the help of circuit simulations. The experimental results are presented in Section IV for prototype circuits fabricated on InP substrates, working in the down-conversion mode at 1.8 GHz.

II. ANALYTICAL TREATMENT

In this section, the basic conversion mechanism for an HITD based mixer is reviewed. It is based on the large-signal–small-signal analysis using conversion matrices [13]. The basic assumption is that the HITD is driven by the local oscillator (LO) signal without involving the negative dynamic region (NDR). This assumption is not strictly regarded as a limitation of the analytical treatment, but a limitation in the actual device operation in order to prevent unstable behavior. The treatment considers the unique feature of the HITD associated with its I/V, i.e., its quasi-square-law behavior around zero bias. The device structure of the diodes under investigation is reported in Table I.

The tunnel diode is square shaped with dimensions 2.5 μm $\times$ 2.5 μm. The intrinsic $I\backslash V$ characteristic for one device is shown in Fig. 1. It is obtained from the measured one after the contribution of a series parasitic resistance Rs of 1.3 Ω is extracted. The value of Rs is calculated using the procedure reported in [17], which is based on the assumption that diodes having different cross sections should have the same peak voltage. It is possible to approximate the I/V characteristics around zero with a polynomial expression. A minimum square-curve-fitting procedure shows that a polynomial equation up to the third degree fits the I/V curve (reported in Fig. 1) in the range $V_D = [-0.2\,\text{V}; 0.2\,\text{V}]$ with a standard error of $3.18e-5$. It is worth noting that this range has been selected because it is symmetric with respect to zero and, on the right axis, is bound by the peak voltage. The result of the approximation is reported in Fig. 2.

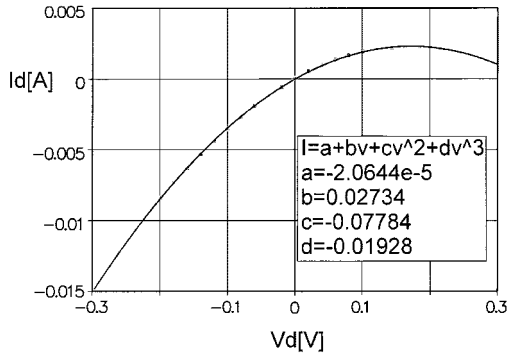

Fig. 2. Approximation by a third degree polynomial of the intrinsic diode I/V around zero bias. The fitting standard error is $3.18e-5$. Symbols: data; continuous curve: fitting.

In the description that follows, a further hypothesis is that the nonlinear capacitance variation can be neglected. This realistic assumption is due to the experimental observation that, for the HITD, the main contribution is due to geometrical capacitance, as discussed in [15], [17], and [18]. Starting from this diode description, the mixing operation can be analyzed by using the equivalent circuit shown in Fig. 3. The impedance $Ze(\omega)$ represents the embedding network and includes the series parasitic resistor Rs, while Is represent the equivalent two-tone excitation

$$I_S(t) = I_S\Big[\sin(\omega_P + \omega_1)t + \sin(\omega_P + \omega_2)t\Big]. \quad (1)$$

The qualitative description of the power of the IM3 component and the conversion loss requires the calculation of the conversion matrix $\mathbf{Y}j$. In the case under investigation and considering the LO signal

$$V_{OL}(t) = V_P \cos(\omega_P t) \quad (2)$$

the conversion matrix assumes the form

$$\mathbf{Y}_J = \begin{vmatrix} b + \frac{3}{2}dV_P^2 & cV_P & \frac{3}{4}dV_P^2 \\ cV_P & b + \frac{3}{2}dV_P^2 & cV_P \\ \frac{3}{4}dV_P^2 & cV_P & b + \frac{3}{2}dV_P^2 \end{vmatrix}. \quad (3)$$

The circuit in Fig. 3 is used for the determination of the potential $V1$, which is the first-order junction voltage, via the conversion matrix technique discussed in [13]. In this case, $V1$ takes the form

$$V1(t) = \frac{1}{2}\sum_{m=-1}^{1}\sum_{\substack{q=-2 \\ q\neq 0}}^{2} V_{m,q}\exp\Big[j(m\omega P + \omega_q)t\Big]. \quad (4)$$

Using the Taylor series expansion, the diode $I\backslash V$ characteristic takes the form

$$I(V) = a + bV + cV^2 + dV^3 \quad (5)$$

where the coefficients are defined in the inset of Fig. 2; retaining the small-signal current up to the third degree, we have

$$i(t) \simeq g_1(t)v(t) + g_2(t)v^2(t) + g_3(t)v^3(t) \quad (6)$$

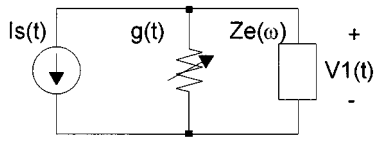

Fig. 3. Time-varying nonlinear equivalent mixer circuit.

where g_2 and g_3 are, respectively,

$$g_2(t) = c + \frac{d}{2}V_p \exp(j\omega_p t) + \frac{d}{2}V_p \exp(-j\omega_p t) \quad (7)$$

$$g_3(t) = d. \quad (8)$$

The calculation of the IM3 component requires the evaluation of the third- and the second-order components of the current source generator $Is(t)$, as indicated in Fig. 3. Once these currents components are determined, the linear conversion matrix analysis can be used to find the voltage across and the current in the embedding impedance at the IM3 frequency.

The second-order current source is expressed as a column vector whose elements are the phasors at the frequency $k\omega_p + \omega_1 - \omega_2$ and $k\omega_p + 2\omega_1$, respectively, $\mathbf{I}_{S,2a}$ and $\mathbf{I}_{S,2b}$, which have the form

$$\mathbf{I}_{S,\,2a} = \begin{bmatrix} I^*_{-1,\,2a} & I_{0,\,2a} & I_{1,\,2a} \end{bmatrix}^T \quad (9)$$

the components are defined by

$$I_{k,\,2a} = \sum_{\substack{h=-1 \\ m+n+h=k}}^{1} \sum_{m=-1}^{1} \sum_{n=-1}^{1} G_{2,\,h} V_{m,\,1} V_{n,\,-2} \quad (10)$$

where $G_{2,h}$ are the Fourier coefficients $g_2(t)$. The second-order voltages are then defined by

$$\mathbf{V}_{2a} = -\mathbf{Z}_{E,\,2a}\left[1 + \mathbf{Y}_j \mathbf{Z}_{E,\,2a}\right]^{-1} \mathbf{I}_{S,\,2a} \quad (11)$$

where $\mathbf{Z}_{E,2a}(\omega)$ is the diagonal embedding matrix at the frequency $k\omega_p + \omega_1 - \omega_2$. Similar equations hold for $\mathbf{I}_{S,2b}$ and $\mathbf{V}_{2b}$.

Analogously are found the third-order current sources components, which are defined by

$$I_{k,\,3} = \sum_{\substack{m=-1 \\ m+n+p=k}}^{1} \sum_{n=-1}^{1} \sum_{p=-1}^{1} G_{3,0} V_{m,\,1} V_{n,\,1} V_{p,\,-2} + \sum_{\substack{h=-1 \\ h+m+n+p=k}}^{1} \sum_{m=-1}^{1} \sum_{n=-1}^{1} G_{2,\,h}\left(V_{m,\,2a} V_{n,\,1} + V_{m,\,2b} V_{n,\,-2}\right) \quad (12)$$

where $G_{3,0}$ is the Fourier coefficient of $g_3(t)$, $V_{m,2a}$, and $V_{m,2b}$ are the second-order voltage coefficients at the $\omega_1 - \omega_2$ and $2\omega_1$ frequencies, respectively.

In conclusion, the third-order current in $Ze(\omega)$ is

$$\mathbf{I}_{E,\,3} = -\left[\mathbf{1} + \mathbf{Y}_j \mathbf{Z}_{E,\,3}\right]^{-1} \mathbf{I}_{S,\,3} \quad (13)$$

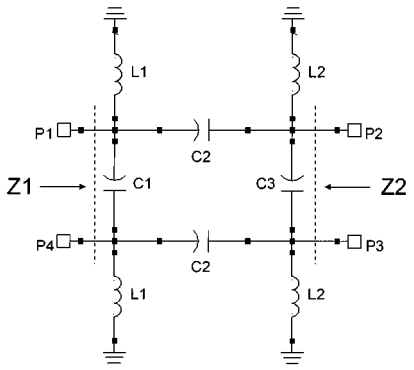

Fig. 4. LEDC topology.

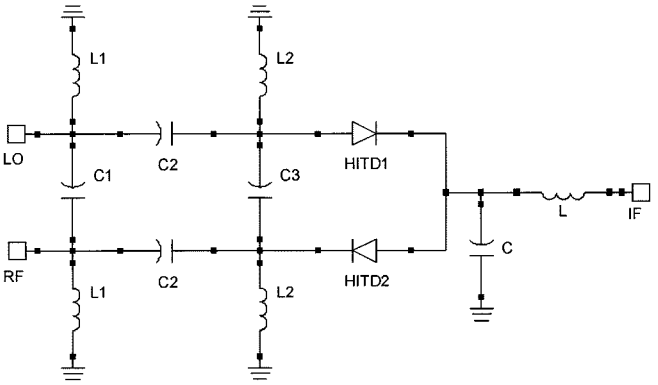

Fig. 5. Single balanced mixer circuit topology.

where $\mathbf{Z}_{E,3}(\omega)$ is the diagonal matrix of the embedding impedances at the third-order mixing frequency. The power dissipated in the embedding impedance at the IM3 component is

$$P_{-1,\,3} = 0.5\left|I_{E;-1,\,3}\right|^2 \mathrm{Re}\{Z_{E;-1,\,3}\}. \quad (14)$$

From (14), it is straightforward to see that the power content at IM3 depends upon the $I\backslash V$ characteristics of the diode. In other words, a low degree of nonlinearity results in a small conversion matrix, i.e., 3×3 in the present case; hence, there are few contributions to the dissipated power in the embedding impedance. Moreover, from it is seen that the first term is directly dominated by the third-order nonlinearity $G_{3,0} = d$. A minimization of this parameter is possible, in principle, through semiconductor bandgap engineering during the HITD development, leading to an effective reduction of the power at the IM3 frequency. This is possible by adjusting the voltage–current pair $(V_{\mathrm{PEAK}}, I_{\mathrm{PEAK}})$. On the circuit design side, from (11)–(14), it is also possible to observe that a reduction of the embedding impedance is required to minimize the IM3 component. We show below how IM3 depends upon the embedding impedance in a particular case of an HITD-based balanced mixer. The mixer uses the LEDC represented in Fig. 4, where the ports 2 and 3 are connected to the diodes; these are then terminated with an arbitrary characteristic impedance $Z2$, which can be selected to reduce the intermodulation (IM) product. The complete mixer schematic is reported in Fig. 5.

The same treatment allows an estimation of the transducer conversion loss L_C for the HITD-based mixer. Considering the conversion matrix in (3), L_C is

$$L_C = \frac{1}{4\left|Y_{j_1,0}\right|^2 \mathrm{Re}\left\{Z_E(\omega_{\mathrm{RF}})\right\}\mathrm{Re}\left\{Z_E(\omega_{\mathrm{IF}})\right\}} \tag{15}$$

where $Y_{j_1,0}$ from results equal to cV_P. Equation (15) shows that L_C depends only on the second degree nonlinearity and that it increases as $Z_E(\omega)$ reduces. A tradeoff between IM3 and L_C is, therefore, required. It is worth noting that c is proportional to the peak current.

III. Design Technique

The LEDC circuit is designed considering as characteristic impedance for two out of the four ports, a value that arises from the tradeoff between the IM3 level, the conversion loss, and the RF/LO isolation. In the particular case of tunnel diodes, the device impedance at zero bias ranges from few tens of ohms to 100 Ω. It depends on the parasitic resistance, the reactive component, and the I/V characteristic around zero. The other ports, i.e., the RF and LO ports, maintain the 50-Ω characteristic impedance of the system. This technique allows tailoring the circuit to the specific impedance requirements of the terminating elements. The LEDC topology is based on two coupled π–LC cells topology [10]–[12], as shown in Fig. 4, where $Z1$ and $Z2$ are the characteristic impedances at ports 1 and 4 and ports 2 and 3, respectively. Introducing the parameters

$$n = \frac{Z1}{Z2} \tag{16}$$

representing the ratio between the system impedance $Z1$ and the impedance associated to the termination $Z2$ and the mean value

$$Z = \sqrt{Z1 \cdot Z2}. \tag{17}$$

The LEDC design formulas can be expressed in the following form [19]:

$$\begin{aligned} C_1 &= \frac{1}{\sqrt{n}\cdot\omega_0\cdot Z} \\ C_2 &= \frac{\sqrt{2}}{\omega_0\cdot Z} \\ C_3 &= \frac{\sqrt{n}}{\omega_0\cdot Z} \\ L_1 &= \frac{Z}{\omega_0\cdot\left(\sqrt{2}+\dfrac{1}{\sqrt{n}}\right)} \\ L_2 &= \frac{Z}{\omega_0\cdot\left(\sqrt{2}+\sqrt{n}\right)} \end{aligned} \tag{18}$$

where ω_0 is the design angular frequency.

The matching problem between the LEDC and nonlinear elements is solved considering that $Z2$ is usually selected to have a value close to the real part of the impedance of the diode biased at $Vd = 0$ V and the residual capacitive part of the diode's impedance is absorbed by the inductor L_2 in the LEDC.

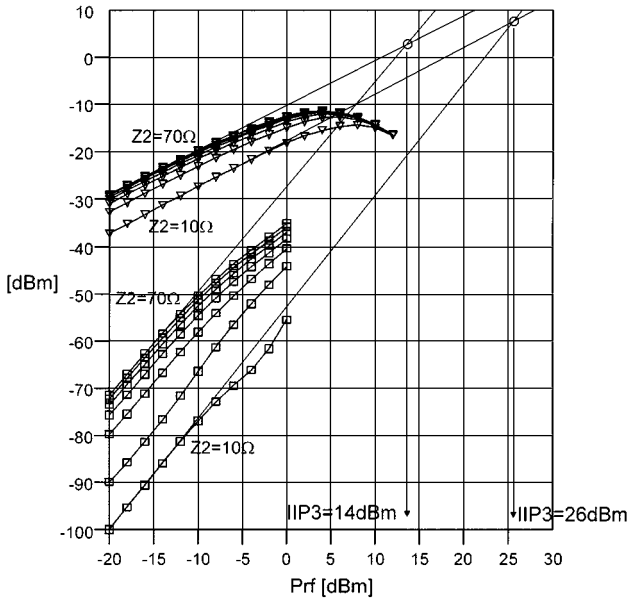

Fig. 6. HITD based balanced mixer output power. IM3 (square) and IF (triangle) for $\mathrm{LO} = 1.8$ GHz, $\mathrm{RF1} = 1.825$ GHz, $\mathrm{RF2} = 1.835$ GHz, $\mathrm{IF} = 25$ MHz, $\mathrm{IM3} = 15$ MHz, $P_{\mathrm{LO}} = 5$ dBm, as a function of $Z2$, ranging from 10 to 70 Ω, step 10 Ω.

The singly balanced mixer shown in Fig. 5 represents the test fixture employed for this investigation. It is composed of, other than the quadrature directional coupler, a couple of identical HITDs and a low-pass IF filter. The latter is a quite simple LC cell, although a proper design should ensure a better RF–LO rejection and a general performance improvement. The component dimensioning is obtained with the intention to fill up the MMIC area left available by the circuit core.

In order to investigate the effects of the terminating impedance $Z2$ on the diode performance, a nonlinear analysis of the balanced mixer has been conducted considering $Z2$ as a simulation parameter ranging from 10 to 70 Ω, step 10 Ω (the results are reported in Fig. 6). In this set of simulations, the HITD is modeled with the intrinsic $I\backslash V$ characteristics reported in Fig. 1 in parallel with an 80-fF constant capacitor and a 1.3-Ω series resistor. These parameter values result from the HITD characterization of a sample fabricated in the same wafer used for the prototype introduced below.

In the analysis, the parasitic components of the LEDC were neglected and the frequencies of interest are $\mathrm{LO} = 1.8$ GHz, $\mathrm{RF1} = 1.825$ GHz, $\mathrm{RF2} = 1.835$ GHz, while the LO power is $P_{\mathrm{LO}} = 5$ dBm and the signal power P_{RF} spans from -20 to 12 dBm. The tone reported in the figure is the intermediate frequency IF at 25 MHz and the IM3 product at 15 MHz. The simulation confirms the theoretical behavior showing a significant reduction of the IM3 level for $Z2 = 10\ \Omega$, while a weaker reduction is observed also for L_C. This is due to the more involved second-order IM and IM3 products dependence from $Z2$, (11)–(14) than the inverse proportionality of L_C from $Z2$ expressed by (15).

For the case under investigation, it is straightforward to see that the third-order intercept point (IIP3) ranges from 14 to 26 dBm depending on the selected embedding impedance. Selecting impedance values in the range of 10–50 Ω results in rather high values for IIP3, making the mixer highly linear. For

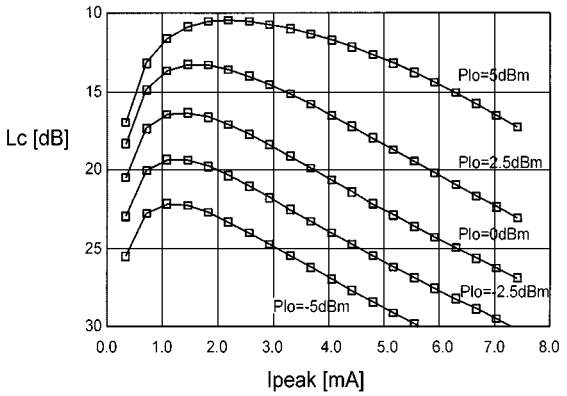

Fig. 7. Conversion loss versus HITD peak current for different LO values.

values of $Z2$ higher than 30 Ω, the insertion loss is less than 10 dB.

The dependence of the conversion loss versus the diode peak current is reported in Fig. 7. For different LO levels and $Z2 = 50\ \Omega$, the peak current spans from 0.36 to 7.5 mA, which is an experimentally determined range. Either scaling the size or changing the doping level can obtain the increases of such a value. In the second case, there is a reduction of the peak–valley current ratio, while the junction capacitance in any case remains within a level that can be easily compensated by $L2$ [20]–[22]. The curves exhibit maximums, which move slightly toward higher current values, as the peak current increases. An increase in the peak current corresponds to a proportional increase of the second degree nonlinearity. This results in a reduction of the conversion loss, as indicated by (15). A further increase results in a mismatch between the LEDC and the HITD pair, which leads to the reduction of the LO and RF power dissipated on the diode. This explains qualitatively the origin of an optimum value of the peak current for a given LO level. It is believed that the unavoidable loss in the LEDC will degrade the conversion mechanism, while the reduction of the series parasitic in the diodes may contribute significantly to a conversion-loss reduction.

Therefore, to design a prototype, the values of the LEDC circuit element have been calculated using $Z1 = 50\ \Omega$ and $Z2 = 35\ \Omega$. The diodes used in the circuit realization have shown very high current densities (50–60 KA/cm^2) and peak–valley ratios between 10–15, [17]–[22]; the selected peak current is 1.8 mA and the LO level is 5 dBm.

The prototype photograph, which is implemented on an InP substrate, is represented in Fig. 8. The entire design, which makes use of the coplanar technology, has been carried out using the Momentum tool available within the Agilent ADS package.[1] This approach allows careful design of the dimensions of any element, and enables the consideration of any electromagnetic coupling between different parts of the circuit, giving further compact arrangement [19]. The overall dimension, including the ground–signal–ground (G–S–G) pads are 1.1 mm $\times$ 1 mm, this can be reduced for higher operative frequency, no more compact solutions are foreseen. The output IF low-pass LC filter introduced on-chip is easily identifiable in Fig. 8.

[1]ADS, EEsof EDA release 1.3, Agilent Technologies, Palo Alto, CA, 2000.

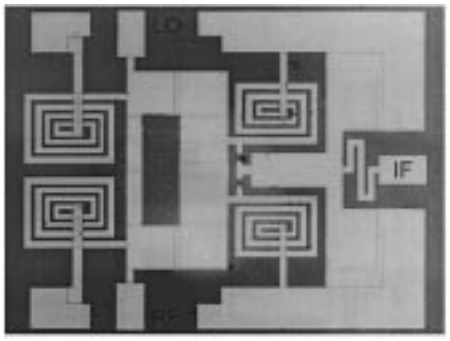

Fig. 8. Prototype chip photograph of the single balanced mixer prototype implemented by LEDC and HITD.

IV. Experimental Results

The simulation data in this section is obtained considering, for the HITD model, the description given in Section III. The small-signal mixer performance in terms of impedance matching, isolation between the RF and LO to IF, and the isolation between the RF and LO are reported in Fig. 9. In the same figure, for the sake of comparison, the simulated performance are also reported. Concerning the RF and LO ports matching [see Fig. 9(a)], a slight frequency shift is observed, which is mainly due to an incorrect guess of the reactive components associated to the actual HITDs. The RF and LO to IF isolation [see Fig. 9(b)] is obtained due to the output IF filter, otherwise this feature would be unachievable. The LO to RF ports isolation [see Fig. 9(c)] is around -15 dB at the design frequency, which is a common value for mixers implemented using 90° coupler. A close investigation of the mixer operation illustrates that the optimization of the linearity performance through a proper choice of $Z2$ may lead to, as a drawback, a mismatch between the LEDC and HITD pair. This results in a signal reflection that reach the input ports, reducing the LO to RF isolation. In any case, this feature can be improved by implementing a 180° coupler.

The large-signal performance of the prototype has been tested using an LO frequency of 1.8 GHz and an RF frequency of 1.83 GHz with different levels of LO and RF power. Fig. 10 shows the mixer performance in terms of IF output power with respect to the LO level depending upon different RF power. From the figures, it is possible to observe that a value of 5 dBm is an acceptable tradeoff between the IF power, linearity, and LO level. In the same figure are also reported the results of a set of harmonic-balance simulation curried out by using the small-signal electromagnetic simulation for the LEDC description, in conjunction with the HITD nonlinear model. The comparison shows a fairly good match between curves for $P_{\rm RF} = 10$ and 5 dBm, while the accuracy of the simulation reduces for $P_{\rm RF} = 0$ dBm, particularly for a low LO level. This may be due to a less accurate polynomial description of the $I\backslash V$ around zero bias.

The main characteristic of the proposed mixer is the linear response, which results in a high value for both the 1-dB compression point and the IIP3 parameters. Fig. 11 reports the IF level as a function of the RF power for 5-dBm LO; this figure permits to evaluate a 1-dB input power compression point of 7 dBm.

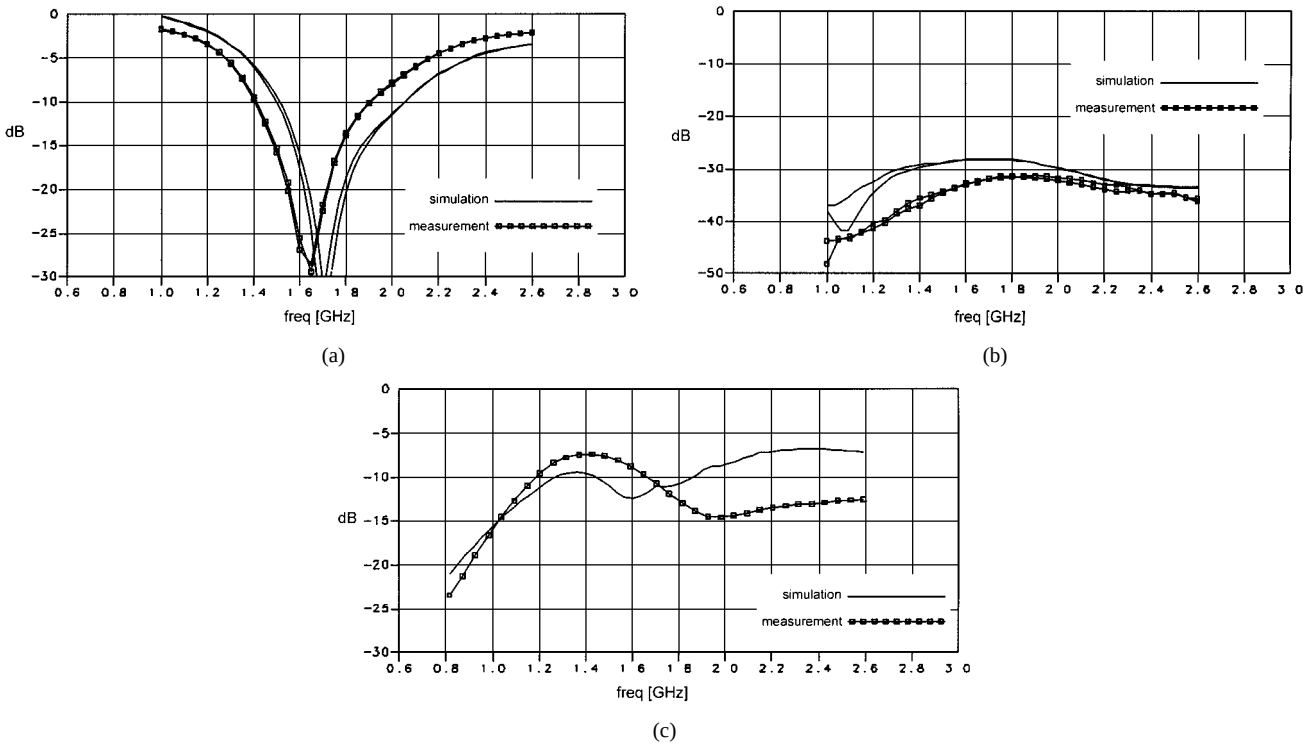

Fig. 9. Small-signal mixer characteristics. (a) RF and LO matching. (b) RF and LO to IF isolation. (c) RF to LO isolation.

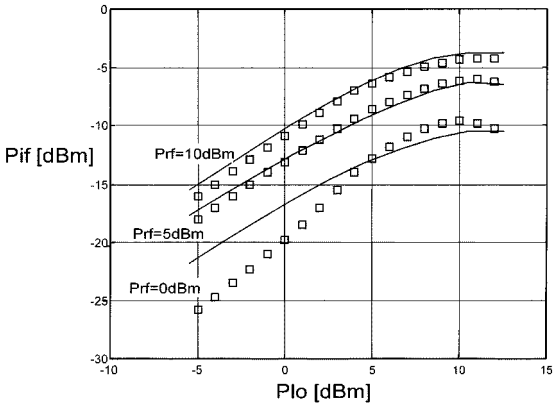

Fig. 10. IF power as a function of LO power at different RF power levels. Squares: measured data, continuous curves: simulations.

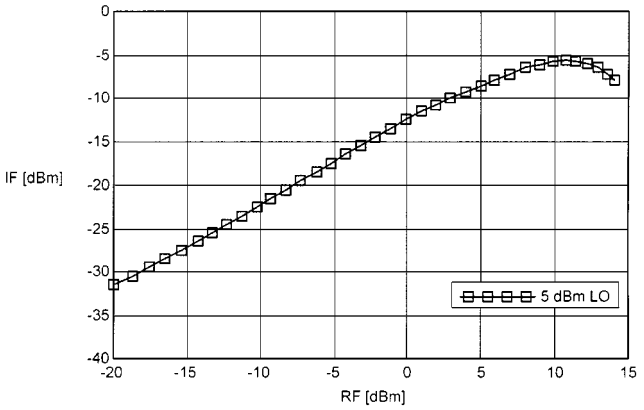

Fig. 11. Output IF power for an input RF frequency of 1.83 GHz and $\mathrm{LO} = 1.8$ GHz. Power level: 5 dBm.

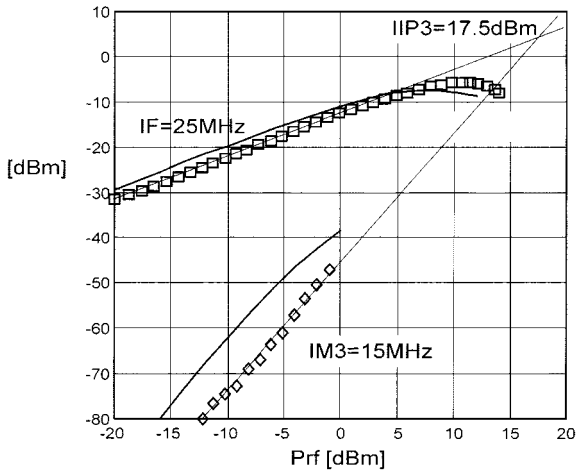

Fig. 12. IF and IM3 output power for $\mathrm{RF1} = 1.825$ GHz, $\mathrm{RF2} = 1.835$ GHz, $\mathrm{LO} = 1.8$ GHz, 5 dBm. The calculated IIP3 is 17.5 dBm. Squares: measured data, continuous curves: simulations.

The linearity of the mixer has been tested using two RF signals at 1.825 and 1.835 GHz, respectively. Fig. 12 plots the IF and IM3 versus the RF input power. The IIP3 is measured and determined as 17.5 dBm under the LO level of 5 dBm. It is worth observing that this performance is usually obtained in double-balanced diode mixers. The same graph reports the simulated data; in this case, the simulation result shows an evaluation of the IIP3 less then the actual value and, again, this could be an effect of the inaccurate description of the odd-order nonlinearities due to the difference in the HITD during the prototype and fabrication and a series resistance underestimation.

In Fig. 13, the rejection behavior concerning the spurious responses $2\cdot\mathrm{RF}+2\cdot\mathrm{LO}$ for $\mathrm{RF} = 1.83\,\mathrm{GHz}$ and $\mathrm{LO} = 1.8\,\mathrm{GHz}$

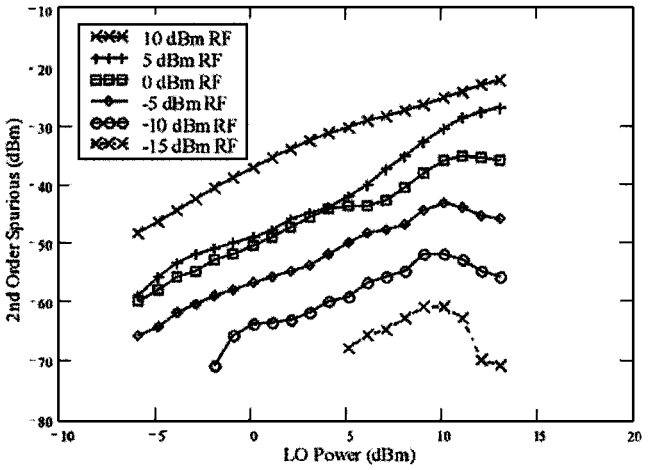

Fig. 13. Spurious response $(2, 2)$ as a function of LO power at different RF power levels. $\mathrm{RF} = 1.83$ GHz, $\mathrm{LO} = 1.8$ GHz.

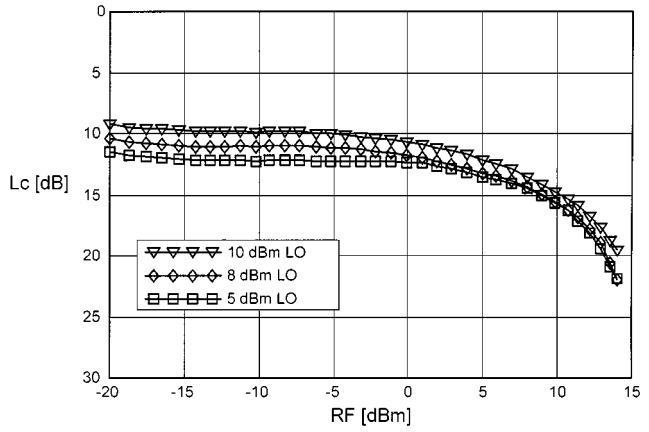

Fig. 14. Conversion loss as a function of the RF power at different LO power levels. $\mathrm{RF} = 1.83$ GHz, $\mathrm{LO} = 1.8$ GHz.

is reported as a function of the LO power for different RF levels. They appear to be more than 20 dB below the IF output level, at the same conditions for the LO and RF input powers, particularly in the case of $+5$-dBm LO and -15 dBm RF; this spurious contribution is 40 dB lower than the respective IF level.

Finally, the mixer conversion loss, shown in Fig. 14, is around 11 dB in the linear behavior range. It varies proportionally to the LO level and remain approximately constant as a function of RF up to -5 dBm. This performance, which is slightly higher than the conversion loss of typical Schottky diode mixers, constitutes the main drawback of the proposed mixer and is due to the low degree of nonlinearity presented by the HITDs. However, as reported in the Fig. 7, this result is very close to the optimum value for the technology. As discussed in [15], the conversion loss, being strongly related to the peak voltage and current presented by the diode, can be further improved by engineering the HITDs $I\backslash V$ shape.

V. Conclusion

A compact single balanced mixer for ISM applications consisting of a tunnel diode biased at 0 V has been described. The diode shows a quasi-second-degree nonlinearity around zero bias. This appears to be an interesting feature for linear mixer development. A prototype working in the 1.8-GHz band has been realized on an InP substrate. Large-signal measurements describe the linear response in terms of both the 1-dB compression point and the IIP3, showing an IIP3 of 17.5 dBm and a 1-dB input power compression point of 7 dB. A series of comparison between measured and simulated data is also reported. In particular, for the small-signal operation, the measured isolation between the input/output ports and matching are compared with simulation carried out with the help of electromagnetic simulation of the passive structure. Large-signal operation measured/simulated data have also been compared, showing a good prevision of the IIP3 and the RF/IF. This study is part of a project aimed to investigate the potential applications of quantum functional devices for MMICs. The extension of such an investigation to higher frequency and the characterization of the noise feature are scheduled future tasks.

References

[1] A. A. Abidi, G. Pottie, and W. J. Kaiser, "Power-conscious design of wireless circuits and systems," *Proc. IEEE*, vol. 88, pp. 1528–1545, Oct. 2000.

[2] S. A. Maas, "How to model intermodulation distortion," in *IEEE MTT-S Int. Microwave Symp. Dig.*, vol. 1, 1991, pp. 149–151.

[3] B. Gilbert, "The MICROMIXER: A highly linear variant of the Gilbert mixer using a bisymmetric class-AB input stage," *IEEE J. Solid-State Circuits*, vol. 32, pp. 1412–1423, Sept. 1997.

[4] M. Chongcheawchamnan and I. D. Robertson, "Linearised microwave mixer using simplified feedforward technique," *Electron. Lett.*, vol. 35, pp. 724–725, Apr. 1999.

[5] S. Peng, P. J. McCleer, and G. I. Haddad, "Nonlinear models for the intermodulation analysis of FET mixers," *IEEE Trans. Microwave Theory Tech.*, vol. 43, pp. 1037–1045, May 1995.

[6] L. Ting-Ping and E. Westerwick, "5-GHz CMOS radio transceiver front-end chipset," *IEEE J. Solid-State Circuits*, vol. 35, pp. 1927–1933, Dec. 2000.

[7] H. Suwaky, T. Nakagawa, and T. Ohira, "An MMIC local oscillator for 16-QAM digital microwave radio systems," *IEEE Trans. Microwave Theory Tech.*, vol. 43, pp. 1230–1235, June 1995.

[8] F. Sabouri, C. Christensen, and T. Larsen, "A single-chip GaAs MMIC image-rejection front-end for digital European cordless telecommunications," *IEEE Trans. Microwave Theory Tech.*, vol. 48, pp. 1318–1325, Aug. 2000.

[9] N. Bourhill, S. Iezekiel, and D. P. Steenson, "A balanced self-oscillating mixer," *IEEE Microwave Guided Wave Lett.*, vol. 10, pp. 481–483, Nov. 2000.

[10] R. W. Vogel, "Analysis and design of lumped- and lumped-distributed-element directional couplers for MIC and MMIC applications," *IEEE Trans. Microwave Theory Tech.*, vol. 40, pp. 253–262, Feb. 1992.

[11] K. Ali and A. Podell, "A wide band GaAs monolithic spiral quadrature hybrid and its circuit application," *IEEE J. Solid-State Circuits*, vol. 26, pp. 1394–1398, Oct. 1991.

[12] G. Avitabile, A. Cidronali, C. Salvador, and M. Speciale, "A compact MMIC 90° coupler for ISM applications," in *IEEE MTT-S Int. Microwave Symp. Dig.*, vol. 1, Denver, CO, June 1997, pp. 281–284.

[13] S. A. Maas, *Nonlinear Microwave Circuits*. Norwood, MA: Artech House, 1988.

[14] D. Coffing and E. Main, "Effects of offsets on bipolar integrated circuit mixer even-order distortion terms," *IEEE Trans. Microwave Theory Tech.*, vol. 1, pp. 23–30, Jan. 2001.

[15] Y. Liu and D. P. D. Steenson, "Investigation of subharmonic mixer based on a quantum barrier device," *IEEE Trans. Microwave Theory Tech.*, vol. 48, pp. 787–763, Apr. 2000.

[16] M. Yu, R. H. Walden, A. E. Schmitz, and M. Lui, "Ka/Q-band doubly balanced MMIC mixers with low LO power," *IEEE Microwave Guided Wave Lett.*, vol. 10, pp. 424–426, Oct. 2000.

[17] A. Cidronali, G. Collodi, M. Deshpande, C. Toccafondi, N. El-Zein, G. Manes, V. Nair, and H. Goronkin, "Modeling and investigation of instabilities in heterojunction interband tunnel diodes for microwave applications," in *IEEE MTT-S Int. Microwave Symp. Dig.*, vol. 2, Phoenix, AZ, May 2001, pp. 1269–1272.

[18] N. El-Zein, M. Deshpande, G. Kramer, J. Lewis, V. Nair, M. Kyler, S. Allen, and H. Goronkin, "DC and RF characterization of different heterojunction interband tunneling diodes," in *Int. Indium Phosphide Related Mater. Conf.*, May 2000, pp. 146–149.
[19] A. Cidronali, G. Collodi, M. Desphande, N. El-Zein, H. Goronkin, G. Manes, V. Nair, and C. Toccafondi, "A MMIC lumped element directional coupler with arbitrary characteristic impedance and its application," in *30th Eur. Microwave Conf.*, Paris, France, Oct. 2000, pp. 374–388.
[20] A. Cidronali, "Stability and tradeoffs of tunnel diodes and their microwave applications, Workshop on 'RF and high speed applications of tunnel devices'," in *IEEE MTT-S Int. Microwave Symp. Dig.*, Phoenix, AZ, May 2001, WCS workshop note.
[21] G. Manes, A. Cidronali, G. Collodi, and C. Toccafondi, "Overview of applications of tunnel diode for high speed integrated circuits, Workshop on 'RF and high speed applications of tunnel devices'," in *IEEE MTT-S Int. Microwave Symp. Dig.*, Phoenix, AZ, May 2001, WCS workshop note.
[22] N. El-Zein and M. Deshpande, "Tunnel diode device simulation and process integration, Workshop on 'RF and high speed applications of tunnel devices'," in *IEEE MTT-S Int. Microwave Symp. Dig.*, Phoenix, AZ, May 2001, WCS workshop note.

Alessandro Cidronali (M'89) was born in Florence, Italy, in 1965. He received the Laurea and Ph.D. degrees in electronic engineering from the University of Florence, Florence, Italy, in 1992 and 1998, respectively.

In 1993, he joined the Department of Electronics Engineering, University of Florence, where he became a Research Associate in 1999. He has been a Lecturer of applied electronics and solid-state electronics courses and currently he teaches a course in microwave electronics. His research activities cover the study of active and passive compact structures for MMICs, the design of multifunction MMICs for low-power wireless applications, computer-aided design (CAD), and numerical modeling of GaAs MESFET and high electron-mobility transistor (HEMT) electron devices. He is currently involved with basic research on quantum functional devices and their applications to microwave circuits.

Giovanni Collodi (M'99) was born in Florence, Italy. He received the Electronic Engineering and the Ph.D. degrees from the University of Florence, Florence, Italy, in 1996 and 2000, respectively.

He then joined the Microelectronic Laboratory, Department of Electronic and Telecommunication, University of Florence, where he is involved in the field of MMIC and millimeter-wave monolithic integrated-circuit (MMMIC) applications. His main interests concern the characterization and modeling of devices for MMMIC and MMIC application, which include circuit design.

Mandar Ramesh Deshpande (M'99) received the Masters degree in physics from the Indian Institute of Technology, Kanpur, India, in 1992, and the Ph.D. degree in physics from Yale University, New Haven, CT, in 1998. His doctoral dissertation concerned electronic transport properties of quantum semiconductor devices.

He is currently with Motorola Laboratories, Tempe, AZ. His current research interests include simulation/modeling and electrical transport characterization of InP- and GaAs-based quantum structures, tunnel diodes, heterostructure FETs (HFETs), and applications of tunnel diodes for RF and microwave circuits.

Nada El-Zein (M'97) received the B.S., M.S., and Ph.D. degrees from the University of Illinois at Urbana-Champaign, in 1990, 1992, and 1995, respectively.

In 1995, she joined Motorola Laboratories, Tempe, AZ, where she has been involved with quantum devices (tunnel diodes) and RF microwave circuits using tunnel diodes or regular HFET devices. Most of this work is done on InP-based materials. Her graduate research was related to semiconductor lasers and related semiconductor devices and effects.

Vijay Nair (M'81–SM'91–F'00) received the M.S. degree in physics and electrical engineering from University of Minnesota, Minneapolis–St. Paul, in 1981.

He is currently with the Physical Sciences Research Laboratory, Motorola Laboratories, Tempe, AZ, where he is currently responsible for development of state-of-the-art devices and monolithic integrated circuits for wireless communication applications. He has authored or co-authored over 50 publications. He holds ten U.S. patents.

Mr. Nair is a member of the IEEE Electron Devices Society, the IEEE Vehicular Technology Society, and the IEEE Microwave Theory and Techniques Society (IEEE MTT-S). He served as the Technical Program Committee (TPC) chairman of the 1997 Radio Frequency Integrated Circuit (RFIC) Symposium and Vehicular Technology Society Conference. He was the general chairman of the 1998 RFIC Symposium. He was also the chairman of the TPC for the 2001 IEEE MTT-S International Microwave Symposium, Phoenix, AZ. He was the recipient of the 1999 Motorola Distinguished Innovator Award, and the IEEE Phoenix section selected him as the 1998 Senior Engineer of the Year.

Gianfranco Manes (M'01) was born in Florence, Italy, on November 16, 1944.

He became an Associate Professor in 1980 and a Full Professor in 1985. He has made contributions in the field of surface-acoustic-wave (SAW) technology for RADAR signal processing and electronic countermeasure (ECM) applications. His major contributions include introducing novel far infrared (FIR) synthesis techniques, fast analog spectrum analysis configurations, and frequency-hopping (FH) waveform synthesis. Since the early 1980's, he has been active in the field of microwave modeling and design. In the early 1990's, he founded and is currently leading the Microelectronics Laboratory, University of Florence, Florence, Italy, which is committed to research in the field of microwave devices. In 1982, he was committed to build up a facility for the design and production of SAWs and microwave integrated circuit (MIC)/MMIC devices, as a subsidiary of the Florence Radar Company SMA Spa. In 1984, the facility became the standalone privately owned microwave company Micrel SpA, which operates in the field of defense electronics and space communications. From 1996 to 2000, he was involved in fourth framework (IV FW) projects in the field of information technology applied to the cultural heritage and he was invited to orientation meetings and advisory panels for the commission. His current research interests are in the field of resonant interband tunneling diode (RITD) devices for microwave applications in a scientific collaboration with the Group at the Physical Science Research Laboratory, Motorola Laboratories, Tempe, AZ. He is the founder and currently President of MIDRA, a research Consortium between the University of Florence and Motorola. He is the Director of the Italian Ph.D. School in Electronics, University of Florence, and in November 2000, he was appointed Deputy Rector for the Information System of the University of Florence. He has authored or co-authored over 100 scientific papers in society journals and presented at international conferences.

Dr. Manes is member of the Board of the Italian Electronics Society.

Herb Goronkin (M'75–SM'83–F'89) received the B.A., M.A., and Ph.D. degrees in physics from Temple University, Philadelphia, PA, in 1961, 1962, and 1973, respectively.

He is currently the Vice President and Director of the Physical Research Laboratories, Motorola Laboratories, Tempe, ZA. Following research assignments in the areas of compound semiconductors, silicon integrated circuits (ICs), optical sensors, and microwave semiconductor devices, he joined Motorola Laboratories in 1977 to build their GaAs electronics program. His laboratory developed Motorola's early versions of heterostructure transistors and circuits for low-power low-noise wireless applications and high-efficiency power transistors for cellular telephones. More recently, his laboratory developed DNA biochips for analysis of genetic defects and spun the effort into a newly formed division in 1998. The laboratory continues development of microfluidic chips for biological sample preparation and analysis. The Physical Research Laboratory, Motorola Laboratories, currently develops quantum and molecular devices for future logic, wireless, and biosensor applications. The Physical Research Laboratory recently transferred its world leadership magnetic random access memory (MRAM) technology to the Semiconductor Products Sector, where there is continued development for product introduction. Motorola's MRAM is based on tunnel junction magnetic devices for universal nonvolatile memory applications. The laboratory also continues the investigation of radical scaling of MRAM memory elements, as well as new device applications of spin-dependent structures and materials. The Physical Research Laboratory is rapidly approaching world parity in the area of molecular electronics, which will be used in future integrated circuits, as well as sensing and analysis of biological molecules. He has authored or co-authored numerous publications and holds over 65 patents.

Dr. Goronkin is a Fellow of the IEEE, a Motorola Dan Noble Fellow, and a member of the American Physical Society and Sigma Xi. He is a member of Motorola's Science Advisory Board Associates. He has served on numerous conference committees and professional organizations. He was the recipient of the 1992 Motorola Distinguished Innovator Award and the 1995 Master Innovator Award. He was selected as the 1993 Senior Engineer of the Year by the Phoenix Section of the IEEE.